Available online at www.sciencedirect.com
SCIENCE DIRECT®
ELSEVIER
Deep-Sea Research I 52 (2005) 647–667
DEEP-SEA RESEARCH PART I
www.elsevier.com/locate/dsr

Retroflections of the North Brazil Current during February 2002

Marlos Goes, Robert Molinari*, Ilson da Silveira, Ilana Wainer

Department of Physical Oceanography, University of São Paulo, Praça do Oceanográfico, 191, Cidade Univeristária, São Paulo, Brazil

Received 3 March 2004; received in revised form 23 September 2004; accepted 7 October 2004
Available online 29 January 2005

Abstract

Retroflections of the North Brazil Current (NBC) are examined using observational data collected in the western tropical Atlantic between 35°W–44°W and 11°S–7°N. Acoustic Doppler Current profiler, conductivity temperature depth oxygen and expendable Bathythermograph data were obtained during a cruise conducted in February 2002. The water column was separated into two layers, the upper layer from the sea-surface to the 24.5 isopycnal and lower layer from the 24.5 to the 26.8 isopycnal. The upper layer includes the NBC, the South Equatorial Current, the North Equatorial Countercurrent (NECC) and a portion of the Equatorial Undercurrent (EUC). The lower layer includes the North Brazil Undercurrent (NBUC), the South Equatorial Undercurrent (SEUC), the North Equatorial Undercurrent (NEUC) and another portion of the EUC. With respect to earlier work, the data show that (1) the SEUC is primarily fed by waters from a recirculation gyre on its northern boundary with some minor transport retroflecting from the NBUC; (2) the EUC is fed primarily by southern hemisphere waters that retroflect from the NBC, but there is some northern hemisphere water in the near surface flow that connects the EUC and NEUC during this cruise; (3) the NECC during this cruise has no connection to the NBC and is fed by northern hemisphere waters originating in the North Equatorial Current; and (4) the majority of the upper layer NBC that crosses 44°W does not appear to retroflect from the boundary farther north to return equatorward. New results include: (1) quantification, for this period, of the amount of transport in the single current core at 44°W that is comprised of waters from the southern (9.2 Sv) and northern hemispheres (5.2 Sv); (2) demonstration that the single core of eastward flow at 44°W and 41°W separates into the NEUC and EUC by 35°W, with the former composed of northern hemisphere waters and the latter southern hemisphere waters; (3) demonstration that the precursor to the EUC (NEUC) at 44°W and 41°W accelerates (decelerates) by 35°W; and (4) depiction of the potential vorticity (PV) field showing that the PV front at 44°W has separated into a front of higher PV values coincident with NEUC and a low PV core at 35°W coincident with the EUC.

Keywords: Western Boundary Currents; Equatorial Undercurrents; Equatorial Countercurrents; Potential Vorticity; Atlantic Ocean; Equatorial

*Corresponding author. National Oceanic and Atmospheric Administration, Atlantic Oceanographic and Meteorological Laboratory, 4301 Rickenbacker Causeway, Miami, FL 33149, USA. Tel.: +1 305 361 4344; fax: +1 305 361 4392.
E-mail address: bob.molinari@noaa.gov (R. Molinari).

0967-0637/$ - see front matter
doi:10.1016/j.dsr.2004.10.010

1. Introduction

The western tropical Atlantic Ocean is a region of extreme importance in inter-hemispheric oceanic exchanges of mass, salt, and temperature. These exchanges play an important role in maintaining the global thermal balance (e.g., Gordon, 1986). Along the western boundary, the cross-equatorial transport occurs in the North Brazil Current (NBC) and the North Brazil Undercurrent (NBUC), Fig. 1. As described in Schott et al. (1998), for example, the NBUC crosses a section at approximately 11°S as a subsurface intensified flow, with a velocity core observed at about 200 m. Between 11°S and the equator, the boundary flow is enhanced by surface intensified transport from the South Equatorial Current (SEC) and the combined flow is now called the NBC (Fig. 1). The NBC continues into the northern hemisphere characterized by a surface velocity core.

Earlier studies of the NBC/NBUC complex found that these western boundary currents are components of the global meridional overturning circulation (MOC), such as in Schott et al. (2002) and Garzoli et al. (2004); the southern hemisphere subtropical cell (STC) (see Snowden and Molinari (2003) for a review of Atlantic STCs); and the wind-driven equatorial gyre, as shown by Mayer and Weisberg (1993). Thus, the dynamics of the NBC/NBUC include a complicated mix of thermodynamics, wind-driven influences and equatorial effects. Similarly, the water mass characteristics of the NBC/NBUC are complex, because of input (1) from the Indian Ocean (the MOC component); (2) subducted in the subtropics of the South Atlantic (the STC component); and (3) circulating in the Sverdrup equatorial gyre.

In addition to participating in inter-hemispheric exchanges, the NBC/NBUC is an important source of mass for many of the near-equatorial zonal currents (Fig. 1). These currents include the South Equatorial Undercurrent (SEUC) and North Equatorial Undercurrent (NEUC) which are both subthermocline currents, located approximately 3–6° from the equator; the Equatorial Undercurrent (EUC) which is located within the thermocline; and the North Equatorial Countercurrent (NECC) which is a surface current, located between 3°N and 8°N.

The EUC, NEUC and NECC are fed by retroflections from the NBC/NBUC at various times, latitudes and depths along the western boundary (e.g., Schott et al., 1995; Bourles et al., 1999a). Schott et al. (1998) hypothesize, based on observations, that the SEUC is not fed by the NBC but rather represents a limb of a large-scale recirculation gyre in the tropical basin. In contrast, Bourles et al. (1999a) indicate that at least a portion of the SEUC does retroflect from the NBUC. There also are differences of opinion on the source waters for the EUC. Bourles et al. (1999a) find no northern hemisphere waters in the EUC, while Schott et al. (1998) do.

Herein, data collected during a February 2002 cruise are used to characterize further the water mass and current structure along the western boundary of the tropical Atlantic. Particular attention will be directed to the characteristics of the various retroflections observed along this boundary. We begin with a description of the data, followed by a discussion of analytical methods. The results are then presented and a summary completes the paper.

2. Data sources and data reduction techniques

The observational data were collected during the Subtropical Cells-2 (STC-2) cruise on the National Oceanic and Atmospheric Administration's R/V RONALD BROWN from February 1 to 24, 2002. Conductivity temperature depth oxygen ($CTDO_2$) stations were occupied along sections at approximately 11°S and 5°S and 35°W and 44°W (Fig. 1). Station depths varied from total water column along the boundary to 2000 m in the interior. Because of time constraints, only expendable bathythermograph (XBT) data were collected on the transects between 35°W and 44°W (Fig. 1). Finally, hull-mounted acoustic Doppler Current Profiler (ADCP) and surface meteorological data were collected continuously along the entire trackline. Data reduction techniques for the observations used in this study are now described.

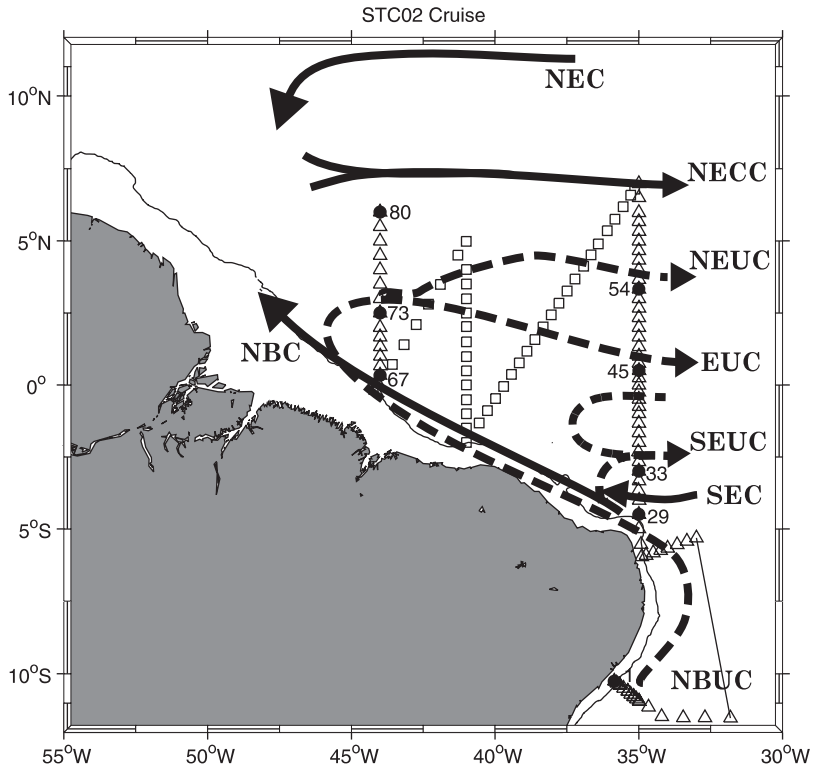

Fig. 1. Locations of CTD (triangles) and XBT (squares) stations occupied during February 2002. Numbers represent CTD stations. A schematic of the surface (solid line) and subsurface (dashed line) currents is superimposed. NBC, North Brazil Current, SEC, South Equatorial Current, NECC, North Equatorial Countercurrent, NBUC, North Brazil Undercurrent, SEUC, South Equatorial Undercurrent, EUC, Equatorial Undercurrent, NEUC, North Equatorial Undercurrent, NEC, North Equatorial Current.

2.1. $CTDO_2$ data

A Sea-Bird 9/11+ $CTDO_2$ unit was used throughout the cruise. A post-cruise calibration of the temperature sensor by the manufacturer indicated that temperature error is negligible. In situ water samples were collected for validation of the oxygen and salinity sensors. The mean difference (standard deviation) between the bottle salinity and calibrated $CTDO_2$ values is .002 (.002) and between the bottle oxygen and calibrated $CTDO_2$ values, .31 (.14) ml/l.

2.2. XBT data

The Mark 12 XBT system was used for the deployment of 44 T-7 XBT's (Fig. 1). The temperature thermister of the XBT is accurate to $\pm 0.15\,^{\circ}C$ and the fall-rate equation used to determine the probes depth, 2% of the depth (Sippican, 1991). Additional in situ verifications of these error estimates were not performed during the cruise. Visual editing of the XBT temperature profiles eliminated erroneous values.

2.3. ADCP data

ADCP observations of currents relative to ship velocity were collected continuously along the track lines. A 150 kHz narrow-band ADCP mounted in the ship's hull was used. The vertical resolution of the ADCP is 8 m with the first data bin located at 17 m below the ship's hull. Data availability should extend to between 350 and 400 m. However, local conditions typically limited the depth range to 300–350 m. Vertical coverage was further limited at the beginning of the cruise to

200 m (the 11°S section). The temporal resolution of the raw data is 5 min.

Absolute velocities were obtained by combining the relative ADCP velocity data with the ship's navigational system (i.e., gyro compass and global positioning system) using a CODAS3 software package (Firing et al., 1995). The absolute velocities were extrapolated to the surface and to 400 m depth, when necessary, using the first and the last reliable ADCP measurements respectively (i.e., the slab layer approximation). The velocity data were then averaged into 15-min bins. The mean standard deviation in these bins is about 2.7 cm/s, which was calculated by averaging horizontally and vertically the standard deviation for all bins.

3. Analytical techniques

3.1. Selection of density surfaces for analysis

To study the NBC/NBUC retroflections, the upper ocean was divided into two layers defined by the isopycnals sigma-$t = 24.5\,kg/m^3$ and sigma-$t = 26.8\,kg/m^3$ (for brevity, the isopycnal units will be omitted when discussing this variable). These isopycnals were chosen as they correspond to the boundaries of important current and water mass cores, are generally located within the depth limits of the ADCP measurements throughout the region, and are equivalent or close to density surfaces used in earlier studies (e.g., Bourles et al., 1999a, Schott et al., 2003). The sea surface to sigma-$t = 24.5$ layer includes the cores of the NBC and NECC (Fig. 2) and for brevity will be called the surface layer. The layer between the 24.5 and 26.8 sigma-t surfaces encompasses the thermocline and subthermocline currents, including the NBUC and NEUC cores and the deeper portion of the EUC (Fig. 2) and will be called the lower layer. The shallower isopycnal is typically found in the velocity core of the EUC (Fig. 2).

3.2. Water mass analyses

Several types of near surface water masses have been identified in the STC-2 region (Bourles et al. (1999a, b), for example). We use property–property curves derived from the CTD data collected in the STC-2 region to distinguish water mass origins (Fig. 3). As in Schott et al. (1995) we chose to average property characteristics from the STC-2 stations that best represent the 3 source regions of water masses: southern (stations 1, 27 and 28, see Fig. 1 for station locations), northern (stations 78, 79 and 80) and eastern (stations 35–38).

Two of these water masses types, northern and southern hemisphere Subtropical Underwater (SUW), form in the subtropics where evaporation exceeds precipitation. The SUW are characterized by a salinity core at about 100 m and are advected westward from their source areas within the subtropical gyres by the NEC and the SEC. Both equatorial currents bifurcate in the western part of the basin, poleward of the STC-2 area, Fig. 1, with one component of each current advecting SUW westward and the other, equatorward.

In the STC-2 region, the southern hemisphere SUW is characterized by higher maximum salinity values and higher oxygen values than it's northern hemisphere counterpart (Fig. 3). Both high-salinity cores overlay the Central Waters, the approximately straight-line portion of the temperature–salinity curve (Fig. 3), of the southern and northern hemisphere. In the study area, North Atlantic Central Water has higher salinity and lower oxygen values than South Atlantic Central Water. Following Bourles et al. (1999b), for brevity, the combination of northern (southern) hemisphere SUW and Central Water will be called North (South) Atlantic Water, NAW (SAW).

Another STC-2 water mass has its source in the eastern tropical Atlantic and is advected into the western tropical Atlantic by the southern edge of NEC and the northern edge of the SEC. In the STC-2 region, this water mass has lower salinities than both SAW and NAW on isopycnals near the salinity maximum. Furthermore, Eastern Atlantic Water (EAW) is characterized by very low oxygen concentrations between about 10 and 15 °C, Fig. 3. Representative oxygen-salinity curves for the three water masses are also given in Fig. 3. These curves will be used to identify the source regions for the water masses observed during STC-2.

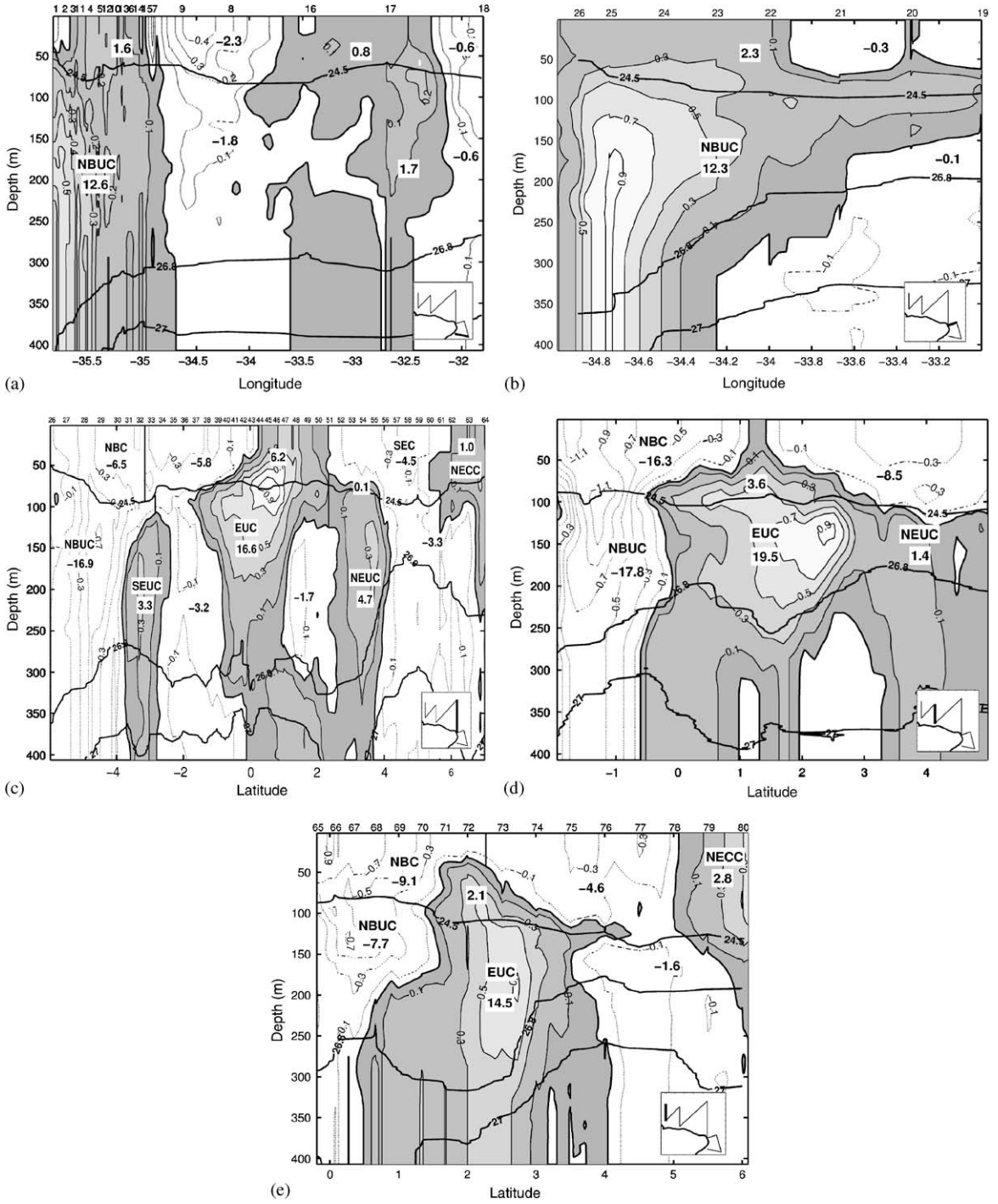

Fig. 2. Vertical sections of the northward component of speed (m/s) for (a) 11°S, (b) 5°S; and eastward component of speed (m/s) for (c) 35°W, (d) 41°W and (e) 44°W transects shown on Fig. 1. The 24.5 and 26.8 isopycnal surfaces and transport of the major currents are also given. NBC, North Brazil Current, SEC, South Equatorial Current, NECC, North Equatorial Countercurrent, NBUC, North Brazil Undercurrent, SEUC, South Equatorial Undercurrent, EUC, Equatorial Undercurrent, NEUC, North Equatorial Undercurrent. Station positions are indicated at the top of each panel.

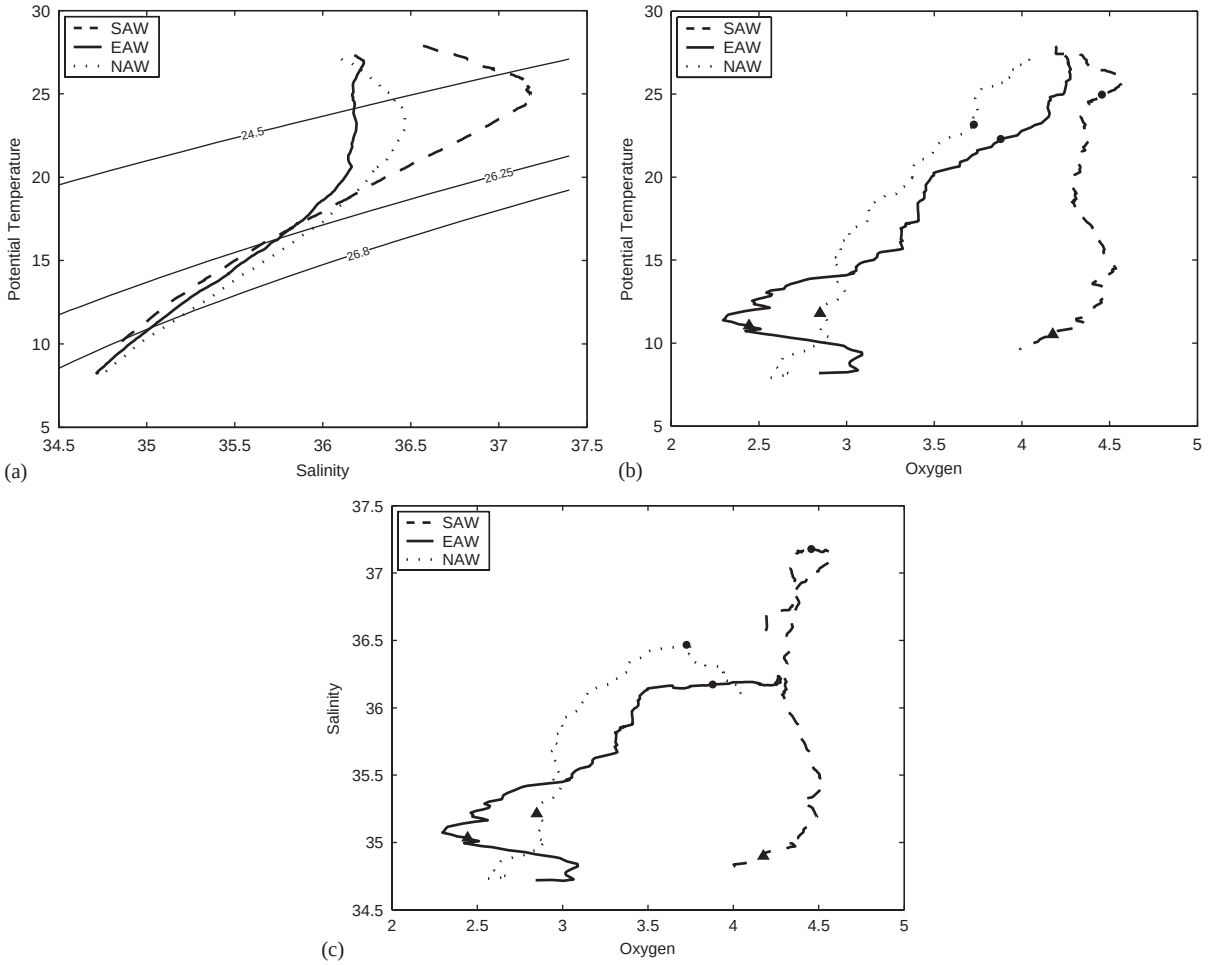

Fig. 3. (a) Theta-salinity, (b) theta-oxygen and (c) oxygen–salinity curves representative of the South Atlantic Water (SAW; stations 1, 25 and 27), Eastern Atlantic Water (EAW; stations 35–38) and North Atlantic Water (NAW; stations 78–80). In (b) and (c), the circles represent the sigma-$t = 24.5$ and the triangles represent the sigma-$t = 26.8$.

3.3. Density estimates from XBT data

The analyses applied in this paper require density values throughout the domain. Thus, it was necessary to match the temperature data from the XBT profiles with appropriate salinity data. The salinity for the XBT stations was estimated from the temperature–salinity properties observed during the cruise, as described previously. First, the mean temperature and salinity relationship was estimated at fixed temperatures from the CTD stations at 35°W and 44°W. Then, salinity values were estimated at the XBT temperature values through linear interpolation. Density values were calculated from the observed temperature and estimated salinities using the equation of state given by Millero and Poisson (1981).

The effect of the salinity estimation on the density calculations is estimated by comparing depths of the 24.5 and 26.8 isopycnals (the density surfaces used to delineate water column layers in the analyses, as described previously) computed from the observed temperature and salinity values from the 35°W and 44°W sections with the depths of the sigma surfaces calculated from the interpolated salinity values. The average difference

between the depths of the sigma-$t = 24.5$ surface is -4.9 m and for the sigma-$t = 26.8$ surface, -3.6 m. There is a spatial pattern to the differences of both surfaces. Maximum contrasts (order 40–50 m) are found closest to the western boundary.

3.4. Objective analyses of data fields

The density and velocity data were interpolated onto a $0.3^\circ \times 0.3^\circ$ horizontal grid using the Objective Analysis (OA) scheme of Bretherton et al. (1976). This grid size was a compromise between data availability and the desire to resolve the baroclinic structures in the region (i.e., even along boundaries the Rossby radius is typically greater than 100 km).

In this scheme, the spatial correlation between the stations is approximated, for simplicity, by an isotropic Gaussian function, although in the observations a quasi-meridional boundary current separates from the coast to feed a quasi-zonal current system. The decorrelation length scale, 3.2°, and the variance error, 0.02, were chosen after several tests established an effective balance between accuracy and resolution. These values were applied in both the scalar and vector schemes as we assume that the flow field is geostrophic and thus the thermal wind relation is respected. The error associated with the OA method for the mapping of the scalar isopycnal surfaces is shown in Fig. 4. The error is greatest between 36°W and 39°W, where the data coverage is reduced (Fig. 1).

A vector OA was used to map the velocity data into a streamfunction (SF) field. The velocities are averaged in each layer and the resulting horizontal velocity field is assumed to be non-divergent in this procedure. This assumption is required because the quasi-synoptic and sparse cruise data would result in unrealistically high vertical velocities if divergence was assumed. However, da Silveira et al. (2000) show that the divergent portion of the flow associated with NBC rings (i.e., the same

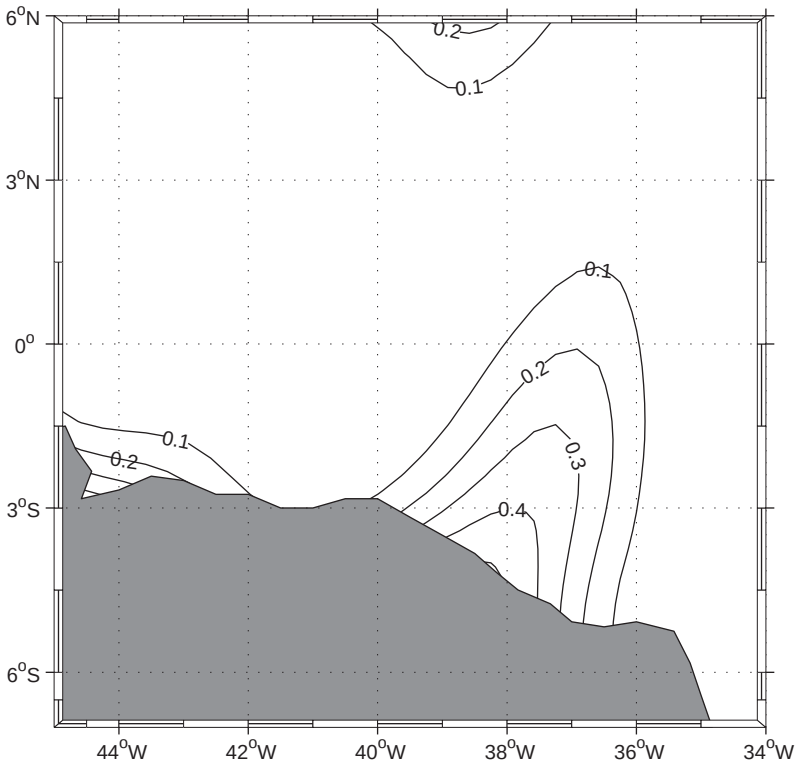

Fig. 4. Normalized root mean square errors associated with the fields gridded by objective analysis.

velocity structure as the NBC itself) is only 10% of the non-divergent component, thus justifying this simplification.

It is further assumed that at the boundary there is no normal flow. To implement this boundary condition, the image method was used. This method consists of approximating the coastline by a series of straight lines and assuming the mirror image of velocity on the landside of the boundary. The interpolation error associated with the vector OA is similar to the scalar uncertainty (Fig. 4) as both only depend on the Gaussian function used to represent the spatial correlations and the data distribution. Additional details on the image method, modifications applied and validation are given in the appendix.

Potential vorticity (PV) fields are then estimated from the SF fields using the Ertel theorem (see Rhines, 1986; Kurgansky et al., 2002 for applications). In an ideal fluid PV is materially conserved which constrains fluid motions and simplifies the analysis (Muller, 1995). The Ertel PV for a layered ocean is given by $\Pi = (\partial v/\partial x \partial u/\partial y + f)/H$, where u and v are the meridional and zonal velocity components, f is the Coriolis parameter and H is the layer thickness. The PV can also be computed using the SF, ψ, as $\Pi = (\nabla^2\psi + f)/H$.

4. Velocity sections, transports and water mass characteristics

4.1. Upper layer

The upper layer current structure of the western tropical Atlantic is complicated in both time and space by the presence of retroflections, equatorial waves (e.g., tropical instability waves), rings, eddies and meanders. For example, Garzoli et al. (2004) compute volume transports for a region just to the northwest of the 44°W section (~47°W) from an array of inverted echo sounders calibrated to estimate the current structure. At this location, they found a range of transports between the sea surface and 300 m during February 2000 of greater than 10 Sv due to the variability of the retroflection position. Similar transport variability can be expected because of the passage of rings, eddies and meanders equatorward of this location. Thus, an exact transport balance is not expected from the STC-2 data collected over a 3-week period. The water mass structure is also complicated by, for example, river discharge (i.e., surface lenses of low salinity from the Amazon River are advected around the NBC retroflection) and precipitation (i.e., the Intertropical Convergence Zone is typically located farthest south in the western Atlantic during boreal winter). Thus, only large-scale, upper layer circulation and water mass characteristics are described.

The northward boundary transport through both the 11°S and 5°S sections in the upper layer is less than 2.5 Sv, 1 Sv = 10^6 m^3/s, (Fig. 2a and 2b). This value is similar to the 2.7 ± 1.8 Sv of upper layer flow at 5°S estimated from 6 sections and using the same lower boundary by Schott et al. (2002). At 35°W (Fig. 2c), the boundary current transport is enhanced to 12.3 Sv by input north of 5°S from the SEC. Schott et al. (2003) computed a mean surface NBC transport of 13.6 Sv from an average of 13 cruises (including STC-2) at 35°W. The SEC waters have lower surface salinities (order 36.2) than the near surface boundary current waters at 11°S (order 36.9), not shown.

The NBC upper layer transport increased from 12.3 Sv at 35°W to 16.3 Sv at 41°W and decreased to 9.1 Sv at 44°W (Table 1). The increase in transport between 35°W and 41°W implies that no waters retroflected from the NBC between 35°W and 41°W. However, this increase in NBC flow is not consistent with the eastward transport of the offshore flow between these two latitudes, which increased from 3.6 to 6.2 Sv (Figs. 2c and 2d), implying a possible augmentation of the flow at 41°W by retroflected waters. Similarly, the 7 Sv decrease in NBC transport between 41°W and 44°W is inconsistent with only a 1 Sv increase in eastward transport between 44°W and 41°W. These inconsistencies can be explained, in part, by the large variability observed in this portion of the water column. In addition, the boundary section might not have covered the entire NBC. For example, Johns et al. (1998) estimate a 3–5 Sv transport for a "continuous coastal boundary current confined over the shelf". This boundary current was not sampled during STC-2.

Table 1
Transports (Sv) of the major currents decomposed by isopycnal layers

Current	Section	$\sigma_0 < 24.5$	$24.5 < \sigma_0 < 26.8$	Total
CSEC	35°W	5.8	3.2	10.0
NBC/NBUC	35°W	6.5	13.7	20.2
	41°W	16.2	17.6	33.8
	44°W	9.1	7.7	16.8
	5°S	2.6	12.3	14.9
	11°S	1.6	12.6	14.2
SEUC	35°W	0	3.3	3.3
EUC	35°W	6.2	16.7	22.9
	41°W	3.5[a]	19.5[a]	23.0[a]
	44°W	2.1	14.5	16.6
NEUC	35°W	0.4	4.7	5.1
	41°W	0[a]	0.8[a]	0.8[a]
NSEC	35°W	4.5	3.2	7.7
	41°W	8.5	—	8.5
	44°W	4.6	1.6	6.2
BC	11°S	2.6	1.8	4.4

CSEC, central branch of the South Equatorial Current, NBC, North Brazil Current, NBUC, North Brazil Undercurrent, SEUC, South Equatorial Undercurrent, EUC, Equatorial Undercurrent, NEUC, North Equatorial Undercurrent, nSEC, northern branch of the South Equatorial Current, BC, Brazil Current.

[a]Only one current core is observed at 41°W (Fig. 2) and the transport of this core is arbitrarily attributed to the EUC at this longitude.

The approximately linear average oxygen–salinity curve observed at the coastal boundary at 11°S, 5°S and 35°W (Fig. 3) is similar to the curves observed on the inshore stations of the 44°W section (stations 70 and 71, Fig. 5). In contrast, however, the near surface layers at 44°W exhibit lower salinity concentrations probably because of the influence of river discharge from South America and/or the high precipitation due to the atmospheric convection at the ITCZ. Stations 71 and 72 include areas of eastward flow (Fig. 2e) with southern hemisphere characteristics ($S > 36.5$; Fig. 5) and a total transport of only 1.1 Sv. Thus only a small portion of the NBC flowing along the boundary at 44°W (9.1 Sv) retroflects west of this latitude to become entrained into the eastward core (Fig. 2e). The remaining NBC transport can retroflect to the northwest of 44°W and not return equatorward and/or continue on along the western boundary into the subtropics of the North Atlantic. The total transport between stations 73–78 is 4.6 Sv westward (Fig. 2e). These

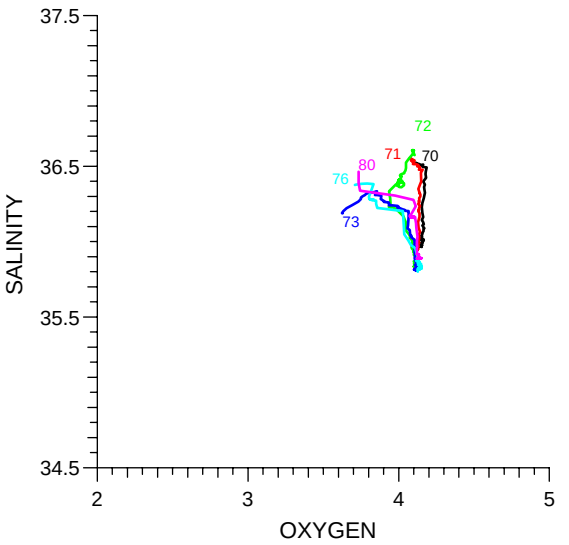

Fig. 5. Oxygen–salinity curves for the layer extending from the sea surface to the 24.5 isopycnal from stations along 44°W. The curve from station 70 is representative of stations 65–69, all in the NBC (Fig. 2). Station numbers are given close to the deepest point of the layer.

waters have NAW characteristics ($S>36.3$, $O_2\sim3.8$; Fig. 5).

The northernmost surface layer zonal flow, the NECC, is inadequately resolved by the STC-2 coverage (i.e., it is only partially sampled at the northernmost stations at 6°N, 44°W and 7°N, 35°W, Fig. 2e and 2c). In contrast to four of the six sections at 44°W presented by Bourles et al. (1999b), during STC-2 the NECC is separated from and north of the subsurface eastward velocity core at this latitude (Fig. 2e). Bourles et al. (1999b) did observe a similar pattern during January 1990 and 1991, that is, a surface intensified NECC separated from the subsurface current core. The NECC is transporting NAW (Station 80, Fig. 5) and thus it appears unlikely that during STC-2 waters that have retroflected from the NBC fed this eastward flow.

4.2. Lower layer

The sections at the nominal latitudes of 11°S and 5°S (Figs. 2a and 2b) are re-occupations of earlier transects reported on by Schott et al. (1995), Stramma and Schott (1996), Bourles et al. (1999a) and Schott et al. (2003), for example. The NBUC appears in all the earlier occupations of the two sections. Thus, consistent with the results from these earlier studies, the NBUC is also present during STC-2 at these latitudes, with a current core close to the boundary at a depth of about 200 m (Fig. 2a and 2b). The earlier results and STC-2 sections provide further evidence that the NBUC is a permanent feature of the circulation along the tropical western boundary.

The total northward boundary transport at 5°S (11°S) between the 24.5 and 26.8 isopycnals is 12.6 (12.3) Sv. It should be noted that some extrapolation is required to obtain these estimates as the lower isotherm extends somewhat deeper then the ADCP coverage (Figs. 2a and 2b). Although increasing the uncertainty in the two estimates, the similarity suggests that there is no significant contribution to or diminution of the boundary flow between the two latitudes in this portion of the water column. Stramma and Schott (1996) also observed similar transports at the two transects.

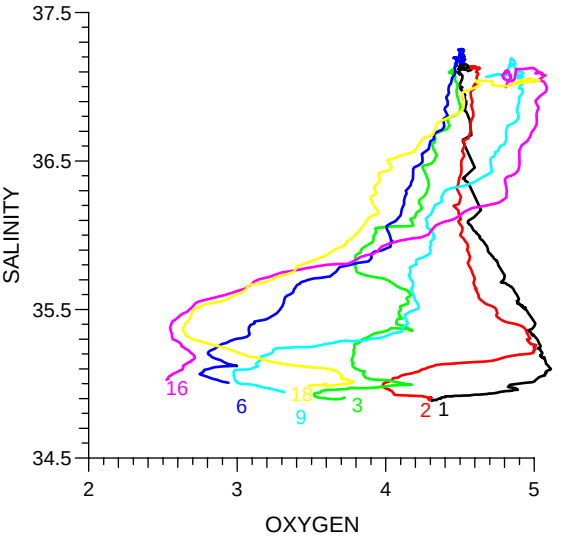

Fig. 6. Oxygen–salinity curves for the layer bounded by the 24.5 and 26.8 isopycnals from stations along 11°S. Stations 1, 2, 3 and 6 are in the NBUC and stations 9, 16, and 18 in the offshore southward flow (Fig. 2). Station numbers are given close to the deepest point of the layer.

Schott et al. (2003) estimated a mean NBUC transport from six crossings of the 5°S section of 13.4 ± 2.5 Sv between the 24.5 and 26.8 isopycnals. The STC-2 transport for this section (12.6 Sv) is thus very close to previous estimates. In the deeper portion of the lower layer, the oxygen and salinity properties transition from the approximately linear oxygen–salinity relation at the boundary (stations 1 and 2, 11°S, Fig. 6) to lower oxygen and salinity, EAW characteristics offshore (stations offshore of station 2, Fig. 6). In the upper portion of this layer, the farthest offshore stations at 11°S (i.e., 9, 16, and 18) are located in southward flow and have increased oxygen concentrations (Fig. 6) that are not found at any other STC-2 stations.

At 35°W, input from the SEC has joined the boundary current. The flow is still characterized by a subsurface velocity core (Fig. 2c), but the NBUC transport has increased to almost 17 Sv (i.e., the SEC contribution to the boundary current extends deeper than the 24.5 isopycnal surface). North of the NBUC, the SEUC flows eastward (Fig. 1). At 35°W, the SEUC transports 3.3 Sv in the lower layer, with another 1.3 Sv advected between the

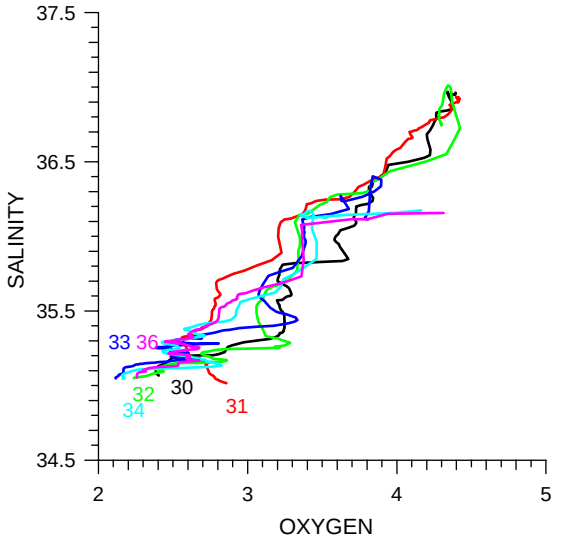

Fig. 7. Oxygen–salinity curves for the layer bounded by the 24.5 and 26.8 isopycnals from stations along 35°W. Station 30 is in the NBC, stations 31–34 in the SEUC and station 36 in the recirculation gyre to the north of the SEUC (Fig. 2). Station numbers are given close to the deepest point of the layer.

26.8 and 27.0 isopycnals, summing to 4.6 Sv for the SEUC transport above sigma-$t = 27.0$. Schott et al. (2003) computed a mean 35°W SEUC transport between 200 and 500 m from 13 sections (including STC-2) of 2.8 Sv. They attribute additional eastward flow below the SEUC to the Southern Intermediate Countercurrent, a distinction we do not make.

The SEUC is located coincident with the southern hemisphere thermostad, indicated by the deepening of the 26.8 surface towards the equator (Fig. 2c). The transition from the boundary flow to the SEUC in oxygen–salinity space is shown in Fig. 7. Schott et al. (2002) note that high oxygen values in the SEUC suggest a western boundary origin for the SEUC. In contrast, however, Schott et al. (1995, 1998) found no connection between the NBUC and the SEUC.

Our results do suggest a minor connection on the southern side of the SEUC with the boundary current. Higher salinity values associated with the boundary flow (station 30, Fig. 7) are observed in the SEUC at stations 31 and 32 in the upper portion of the lower layer. However, the transport of these boundary flow waters in the SEUC is less than 1 Sv.

Less saline water is observed in the upper portion of the lower layer at stations 34 and 35 (Fig. 7). These lower salinities and the lower oxygen and salinity concentrations observed deeper in the 24.5–26.8 layer at all the stations within the SEUC (Fig. 7) are representative of EAW (see Fig. 3). Schott et al. (1995, 1998) find that the EAW is advected westward in the northern limb of a basin wide recirculation gyre. In their circulation schematic, the SEUC is the southern limb of the gyre. Station 36 is located in the westward flow (Fig. 2) and has water mass characteristics similar to those in the SEUC (Fig. 7) supporting the hypothesis of Schott et al. (1995, 1998).

No CTD data were collected along the 41°W transect (Fig. 4d) because of time constraints. The boundary flow at this longitude is surface intensified because of the addition of SEC transport to the NBUC and is now designated the NBC (e.g., Schott et al., 1995). The NBC transport in the lower layer is essentially the same as at 35°W (17.8 versus 16.9 Sv, Fig. 4c). This similarity in the lower layer transport supports the previous suggestion that only a very small portion of the NBUC retroflects to feed the SEUC.

The NBC transport in the lower layer has decreased 10.1 Sv between 41°W and 44°W (Fig. 2d and 2e). However, the transport of the cores of eastward flow at these two longitudes differs by only 6.4 Sv. Thus, it must be considered that the NBC transport at 44°W (7.7 Sv) could underestimate the total boundary current because of possible flow shoreward of 400 m the depth of the inshore station, number 65 (Fig. 2e). Conversely, the total NBC transport above the 26.8 isopycnal is 16.8 Sv, which is very similar to the 16 ± 2 Sv mean NBC transport reported on by Garzoli et al. (2004).

The eastward flow at 44°W has one core with the velocity maximum located at ~2.7°N between 100 and 250 m and a transport of 14.5 Sv (Fig. 2e). The northern hemisphere equatorial thermostad is located between 2°N and 3°N coincident with the location of the speed core on this section. Bourles et al. (1999b), for example, have also observed one current core of eastward flow at 44°W that is

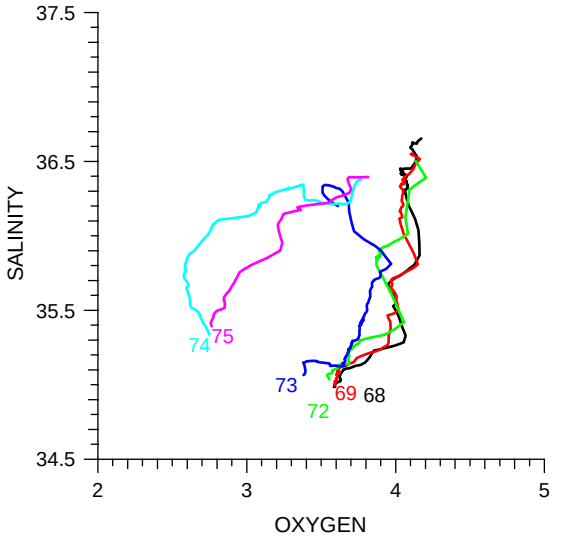

Fig. 8. Oxygen–salinity curves for the layer bounded by the 24.5 and 26.8 isopycnals from casts along 44°W: the curve from station 68 (in the NBC) is representative of the curves from stations 65–67, also in the NBC. Stations 69–75 are in the core of eastward flow at 44°W (Fig. 2). Station numbers are given close to the deepest point of the layer.

comprised of waters from both the northern and southern hemispheres.

Stations 65–68 are within the NBC in the lower layer (Fig. 2e). Water mass properties at these stations are characteristic of southern hemisphere waters (i.e., an approximately linear oxygen–salinity curve in the lower layer, station 68, Fig. 8). The flow at stations 69–75 includes eastward components (Fig. 2e). Water mass characteristics at stations 71 (not shown) and 72 (Fig. 8) are similar to those of the inshore stations in the NBC (i.e., higher oxygen concentrations ~4 ml/l). Thus, a portion of the SAW in the lower layer of the NBC that has crossed 44°W has retroflected northwest of this latitude to return equatorward.

Station 73 (Fig. 8) appears to lie in a transition region between SAW and NAW with the upper portion of the layer exhibiting salinity–oxygen properties similar to those to the north (O_2~3.6 ml/l, S~36.1) and the lower portion, properties similar to those to the south (O_2~3.8 ml/l, S~35.1). Northern hemisphere salinity–oxygen properties (O_2~2.8 ml/l, S~36.1) are observed north of station 74 (Fig. 8). The 14.5 Sv of eastward flow at 44°W is thus comprised of both SAW (9.2 Sv, stations 69–72 and half the transport of station 73, i.e., station 73 is comprised of SAW and NAW and a somewhat arbitrary transport decomposition of 50% of each water mass was made) and NAW (5.3 Sv, stations 74, 75 and half the transport of station 73).

At 44°W, there is a secondary eastward velocity core centered on the 24.5 isopycnal surface and 2.25°N (Fig. 2e). At 41°W, there is an equatorward extension of higher velocities on the 24.5 surface (Fig. 2d). The main subsurface core is located entirely within the lower layer, coincident with the thermostad (Fig. 2d). By 35°W, the velocity cores of the NEUC and EUC have separated. However, there is a shallow region (~100 m) of continuous eastward flow connecting the two speed extremes (Fig. 2c). The NEUC core, located coincident with the thermostad, exhibits lower speeds than the similar core at 41°W. However, the EUC core has higher speeds than it's apparent precursor at 41°W.

The total transport of the EUC, including the eastward flow in the upper layer, is 22.8 Sv at 35°W, Table 1, Fig. 2c. Schott et al. (2003) computed a mean transport for the EUC at 35°W from 13 sections (including STC-2) of 20.9 Sv, including 8.6 Sv above the 24.5-isopycnal surface. Thus, the EUC transport during STC-2 is quite similar to the Schott et al. (2003) average.

Stations 39–48 are in the EUC at 35°W (Fig. 2c). Water mass properties at these stations (shown for stations 41, 43 and 46, Fig. 9) include the characteristic high oxygen concentrations of SAW in the NBC and eastward core at 44°W (e.g., stations 68–72, Fig. 9). Deeper in this layer the properties at station 41 are characteristic of EAW (i.e., oxygen ~2.5 ml/l at sigma-t = 26.8, Fig. 9) and at stations 42–48 (shown for stations 43 and 46, oxygen between 2.8 and 3.4 ml/l at sigma-t = 26.8, Fig. 9). Within the shallow layer connecting the EUC and NEUC (Fig. 2c), NAW properties are observed (station 49, Fig. 9).

The eastward transport of SAW for the 35°W (44°W) stations 36–47 (69–72) is 15.8 Sv (9.1 Sv). Only a small portion of the eastward flow at the easternmost section is comprised of EAW (i.e.,

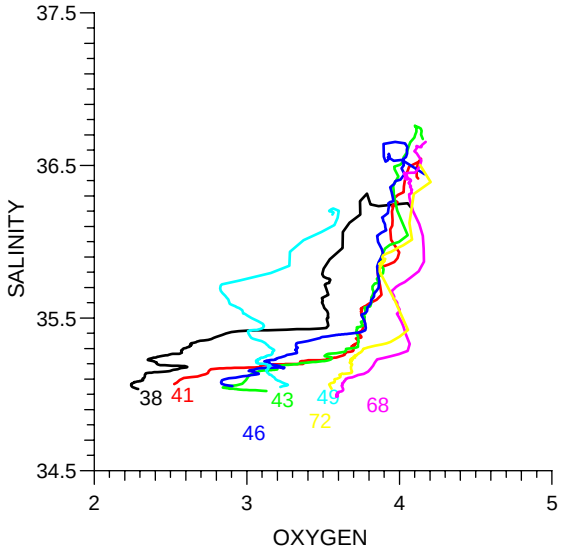

Fig. 9. Oxygen–salinity curves for the layer bounded by the 24.5 and 26.8 isopycnals from casts along 44°W (station 68 in the NBC and 72 in the eastward core, Fig. 2) and 35°W (station 38 in the recirculation gyre and 41, 43, 46, and 49 in the EUC, Fig. 2). Station numbers are given the close to the deepest point of the layer.

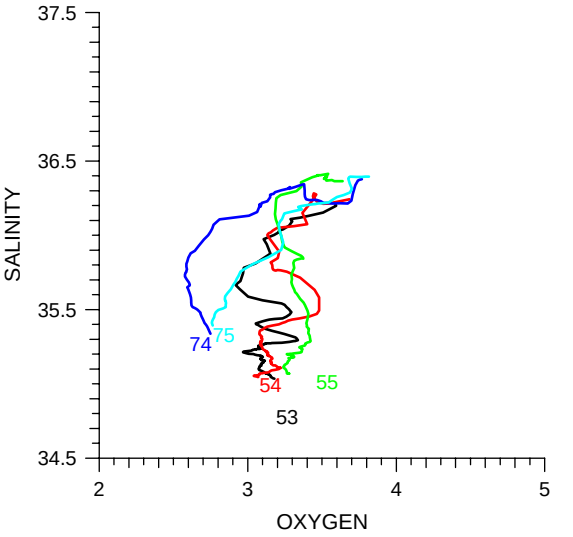

Fig. 10. Oxygen–salinity curves for the layer bounded by the 24.5 and 26.8 isopycnals from casts along 44°W (stations 74,75, in the eastward core, Fig. 2) and 35°W (stations 53, 54, and 55, in the NEUC, Fig. 2).

station 41, Fig. 9). Discounting this minor transport, the difference in SAW transport between the two sections is approximately 6 Sv. This difference lends credence to a retroflection of NBC transport between 35°W and 44°W of about 6 Sv.

The NEUC at 35°W is comprised primarily of NAW ($S<35.5$, $O_2{\sim}3.1$ ml/l), as seen in the stations 53–55 in Fig. 10, with similar characteristics to the stations on the northern side of the eastward flow at 44°W (stations 74–75, Fig. 10). The transport of the NEUC is 4.7 Sv at this longitude, approximately equivalent to the NAW transport of 5.3 Sv in the single eastward core at 44°W. The NEUC core is co-located with the thermostad at 4°N, consistent with earlier studies (Cochrane et al. (1979), for example). Based on their 13 section average, Schott et al. (2003) note that, "The existence of the NEUC is more uncertain at 35°W than that of the SEUC". However, Molinari et al. (2003) in a subset (6 sections) of the 13 transects at 35°W considered by Schott et al. (2003) find a mean NEUC with a 5.4 ± 2.1 transport. The Molinari et al. (2003) NEUC core was located between 4°N and 6°N. The Schott et al. (2003) transect only extends to 5 °N and meridional migration of the NEUC at these latitudes probably accounts for a weaker mean subsurface current core in their calculations.

4.3. *Decomposition of the NBC into its thermohaline, wind driven and STC components*

A qualitative decomposition of the NBC into its thermohaline, wind driven and STC components can be made for the STC-2 cruise period using the cruise data and results from earlier studies. Johns et al. (1998) estimated a mean thermohaline transport from current meter records collected in the NBC at approximately 4°N and 50°W. They assumed that the minimum in the observed mean annual transport (i.e., April–May) represents the thermohaline circulation. The majority of this transport of 8 Sv was in the upper 100 m. This value is close to the 6 Sv estimate of thermohaline transport determined by Zhang et al. (2003) from hydrographic data for the layer above the 26.2 isopycnal.

We assume that about 4 of the 6.5 Sv of NBC and 2–4 Sv of NBUC transport through 35°W

(Fig. 2) is the February, 2002 equivalent of the 6–8 Sv of thermohaline flow estimated by Johns et al. (1998) and Zhang et al. (2003). This STC-2 transport represents additions to the boundary flow by the SEC, which extends across the South Atlantic from the tip of Africa (e.g., Tsuchiya, 1986), that is, a component of the upper limb of the thermohaline circulation.

Johns et al. (1998) also provided an estimate of the mean annual cycle of the transport of the equatorial Sverdrup gyre derived from the linear model of Anderson and Corry (1985). The wind-driven transport February was approximately 5 Sv. We attribute the 5.8 Sv of upper layer SEC transport (Fig. 2c) that is characterized by low salinities originating in the eastern Atlantic (e.g., Merle, 1978) to the Sverdrupian equatorial gyre (i.e., this portion of the SEC represents the southern boundary of the equatorial gyre).

Finally, Zhang et al. (2003) argue from their analysis of hydrographic data that 6 Sv of the southern hemisphere STC flows along the western boundary. The high-salinity values of the NBUC (Fig. 3) are consistent with waters subducted in the subtropical Atlantic that flow equatorward in the STC. Thus, 6 Sv of the STC-2 NBUC transport of some 12 Sv at 11°S and 5°S (Figs. 2a and 2b) are attributed to the STC flow as in Zhang et al. (2003). This leaves the source of some 6 Sv of NBUC transport unaccounted for.

5. Horizontal distributions of streamfunction and potential vorticity

The SF fields for the two layers are given in Fig. 11. These fields, as well as those for PV, have large uncertainties between 40°W and 36°W, and the continental boundary and the equator, because of the absence of data (Fig. 4). At 35°W, the SEC in the upper layer is depicted as a wide westward flow extending from about 6°S to the equator. The SEC merges into the NBC, which then accelerates as indicated by the constriction of the SF contours at 44°W (i.e., the width of the NBC is only 3° at 44°W, Fig. 11). In the lower layer encompassing the NBUC, a similar acceleration is not apparent along the boundary.

The upper layer SF field indicates little retroflection of the boundary current in the STC-2 area, somewhat inconsistent with the transports shown on the vertical sections of Fig. 2, which indicate a 7 Sv reduction in transport between the two westernmost sections. However, as indicated above, a portion of this imbalance could be made up by an unresolved shelf flow. Strong eastward flow is only observed in the eastern portion of the STC-2 region, in the area of the surfacing of the EUC (Fig. 11).

The upper layer SF field depicts almost no eastward flow through 44°W. Thus, the near surface component of the NBC either continues on as throughflow into the northern subtropics and/or retroflects farther north with no eastward return along the western boundary. da Silveira et al. (2000) consider the circulation northwest of the 44°W transect, also using direct velocity observations to estimate SF and PV fields. They use a three-layer model to approximate the vertical structure of the ocean, with the upper layer at rest 150 m thick (i.e., this layer includes the NECC) and the middle layer 850 m thick (i.e., this layer includes the NEUC). Their upper layer SF distribution for January 1991 shows a retroflection of the NBC west of 44°W between 5°N and 7°N. These retroflected waters turn northwestward and cross 44°W between 6°N and 9°N (i.e., outside the area of STC-2, Fig. 11). Thus, similar to the February 2002 pattern, none of the retroflected transport returns equatorward close to the western boundary.

In contrast to the absence of significant upper layer offshore flow, there is considerable retroflection of the lower layer boundary flow between 41°W and 44°W (Fig. 11), again consistent with the transports described previously. There is also indication of equatorward flow through the 44°W transect joining these retroflected waters in a single core. The eastward core crosses the 41°W section and a portion of this flow then spins-off and flows north (Fig. 11). This splitting of the single eastward core occurs in the same region, 40–35°W, indicated by the acceleration potential distribution for the February–April season constructed by Cochrane et al. (1979). Their presentation shows this separated flow then turning

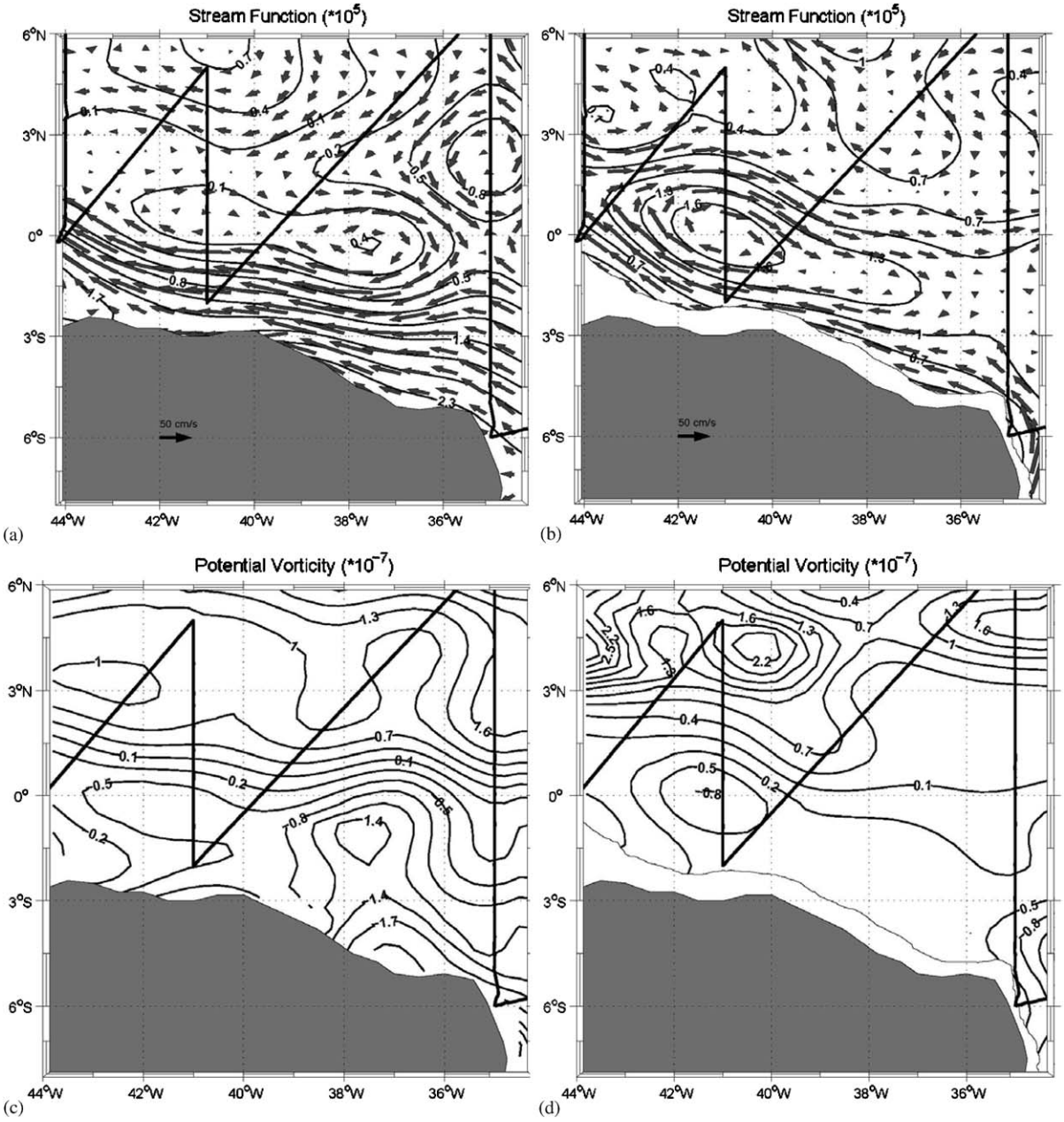

Fig. 11. Upper panels: Stream function fields for the upper, right panel (lower, left panel) layer bounded by the surface and 24.5 (24.5 and 26.8) isopycnal surfaces. Lower panels: Potential vorticity fields for the same layers.

eastward between about 4°N and 7°N to become the NEUC.

The splitting of the single core at 44°W and 41°W into the NEUC and EUC was inferred from the sections given in Fig. 2 and the water mass characteristics described previously. However, the SF distribution in Fig. 11 depicts the majority of the northward branch of the eastward core leaving

the region through 6°N. The NEUC in the SF field is fed primarily by southward flow entering the region through 6°N. However, there is the potential for some of the NEUC to be fed by flow on the north side of an eddy centered at about 3°N and 37.5°W (Fig. 11). This path would be consistent with the path inferred from the Cochrane et al. (1979) acceleration potential field. The data distribution and temporal variability of the region limits the ability of the OA scheme to reproduce exactly the flow field.

The intrusion of the NBC is marked in both layers by a zone of low PV extending into the northern hemisphere (Fig. 11). The low PV region between 36°W and 38°W, located from the boundary to the equator, are in a region of no data and thus suspect. However, the low PV values either side of this feature are located in areas of data (Fig. 11). PV values less than -0.4×10^{-7}/s extend through the 44°W transect in the upper layer, while only 0 PV contours reach the 44°W transect in the lower layer. These PV patterns, as were the SF patterns, are similar to the January 1991 fields of da Silveira et al. (2000); low PV values extend farther north in their upper than lower layer.

In the western portion of the STC-2 area, a PV front is observed just north of the equator in both layers, consistent with the results of da Silveira et al. (2000). In the upper layer, this front is continuous and slopes equatorward towards the east (Fig. 11). In the lower layer, this front is continuous to east of 41°W, where higher PV values separate from the front and turn northward, as do the currents (Fig. 11). The northern PV front turns eastward between 3°N and 4°N, crossing 35°W at the same latitude as the NEUC.

6. Summary

As indicated throughout the previous text, many of the results presented herein have been described in earlier works from data collected in different time periods. However, as will now be summarized, we have been able to present results that (1) add more information to corroborate the earlier studies; (2) address open questions, and/or (3) provide new quantitative results. Examples from each of these categories are now given.

Additions to and corroboration of earlier findings:

- The NBUC was observed on the 11°S and 5°S transects during STC-2, consistent with earlier work such as Schott et al. (2002). The upper (lower) layer transports of the NBUC at 5°S, 2.6 (12.3) Sv, are close to the 6-cruise averages given in Schott et al. (2002) of 2.7 ± 1.8 (13.4 ± 2.7) Sv. The presence of the NBUC in all the occupations of these sections and also in the numerical model used in Schott and Boening (1991) work lend credence to the hypothesis that the NBUC is a permanent feature of the western boundary circulation (e.g., Schott et al., 2002).
- There is little change in the transport of the NBUC layer between 11°S (12.6 Sv) and 5°S (12.3 Sv) during STC-2 and other cruises that occupied these sections (e.g., Stramma and Schott, 1996).
- The SEC joins the boundary flow north of 5°N and transforms the subsurface intensified NBUC to the surface intensified NBC west of 35°W. During STC-2, the SEC added 10 Sv to the upper layer boundary flow, comparable to the 12 Sv found by Schott et al. (1995) during March 1994.
- The SF and water mass distributions show that different layers of the NBC can retroflect at different latitudes, as observed previously (e.g., da Silveira et al., 2000). During STC-2, a large portion of the lower layer retroflected close to 44°W (Fig. 11) and returned SAW equatorward to feed the EUC (Fig. 9). As indicated by water mass characteristics, if the upper layer retroflected, the associated transport did not return equatorward. da Silveira et al. (2000) described the January 1991 current structure along the boundary west of 44°W and generated SF distributions that showed the NBC did indeed retroflect northwest of this transect with the resulting transport continuing to the northeast rather than returning equatorward.
- The intrusion of the NBC in both layers is marked by the extension of low PV contours

into the northern hemisphere as in da Silveira et al. (2000) for a January 1991 cruise.
- The single core of lower layer eastward flow at 44°W and 41°W splits into the NEUC and EUC by 35°W. Cochrane et al. (1979) first observed this pattern using a composite potential acceleration distribution generated from late winter-early spring cruises.
- Surfacing of the EUC is consistent with earlier findings of this feature during this season (e.g., Schott et al., 2003). Although the surface velocities are extrapolated from about 25 m, the water mass characteristics of the surface flow above the EUC argue for a connection to the lower layers (i.e., the upper and lower layer water mass characteristics are SAW).
- Transports for the various currents considered are summarized in Table 1. As indicated in previous sections, these estimates fall well within the range of earlier studies.

Address open questions:

- As determined by water mass characteristics (Fig. 7), during February 2002, the SEUC is fed by both a small contribution from a partial retroflection of the NBUC and primarily a recirculation gyre located to the north of the zonal flow (Fig. 1). The SEUC represents the southern branch of the recirculation gyre. This finding supports previous studies, which observed high oxygen concentration in the SEUC (i.e., a boundary source, Tsuchiya, 1986) but is in contrast to other work, which only found a recirculation source (e.g., Schott et al., 1995, 1998). Obviously, temporal variability can result in both patterns occurring at different times.
- The majority of the EUC transport is comprised of SAW mixed with EAW (Figs. 8 and 9). The only NAW is found in the thin layer of eastward flow that connects the EUC and NEUC (Figs. 2 and 9). It can not be determined from these data if this NAW remains with EUC and/or the NEUC. Several earlier studies have found no evidence for NAW in the EUC (e.g., Schott et al., 1995; Bourles et al., 1999a).
- The NECC is completely separate from the subsurface eastward core to the south at 44° W as observed in previous studies. There is no contribution of SAW to the NECC during this cruise similar to observations during other late-winter early spring cruises (i.e., there is no NBC, only an NEC contribution to the NECC as observed by Bourles et al. (1999a, b), for example). The representativeness of this structure as a component of the annual cycle remains an open question because of the limited number of cruises available for study.
- The decomposition of the NBC into its thermohaline, wind driven and STC components was made for the STC-2 period. We attributed 5.8 Sv of NBC flow at 35°W contributed by upper layer SEC transport (Fig. 2c) to the equatorial Sverdrup gyre upper layer, 4–6 Sv of upper layer NBC transport to the thermohaline circulation, and 6 Sv to STC flow.

New results:

- This cruise provides quantification of the contributions of the various water masses to the major currents. The SAW transport in the eastward core at 44°W is 9.1 Sv. This is joined by 6 Sv of NBC flow that has retroflected between 41°W and 44°W to form the EUC at 35°W with an SAW transport of 15.2 Sv. The 5.3 Sv of NAW flow in the eastward core at 44°W has separated from that current to become the NEUC with a transport of 4.7 Sv at 35°W.
- At the core level of the EUC, the flow accelerates between 41°W and 35°W, while at the core level of the NEUC the flow has decelerated between these sections.
- The PV field depicts the separation of the NEUC and EUC cores east of 41°W. The NEUC core is characterized by higher PV values indicative of a northern hemisphere source and the EUC core, by lower PV values indicative of a primarily southern hemisphere source. Although depicted in potential acceleration distributions by Cochrane et al. (1979), we are unaware of any previous PV fields that show this separation.

Remaining questions:

- What are the respective roles of NBC transport (e.g., Garzoli et al., 2004) and PV distribution (Fig. 11) in determining the retroflection latitude of the upper and lower layers?
- What are the dynamics of the separation of the single eastward core at 44°W and 41°W into the NEUC and EUC at 35°W?
- Why does the layer at 41°W that becomes the EUC at 35°W accelerate and the layer that becomes the NEUC decelerate between the two sections?
- What portions of the NBC/NBUC transport are derived from the thermohaline circulation, from the southern hemisphere Subtropical Cell and from the Sverdrup equatorial gyre on annual time-scales?
- What dynamics control the recirculation gyre and its southern boundary, the SEUC?
- How representative of late winter early spring circulation patterns were the STC-2 features?

Acknowledgments

We gratefully acknowledge the outstanding performance of the officers and crew of the RON BROWN during STC-2. Valuable comments by Dr. Silvia Garzoli and two anonymous reviewers are appreciated.

Appendix A. The image method and validation

The image method was developed in three steps:

(1) This first step is subjective. The points where the images are located are chosen in a way that

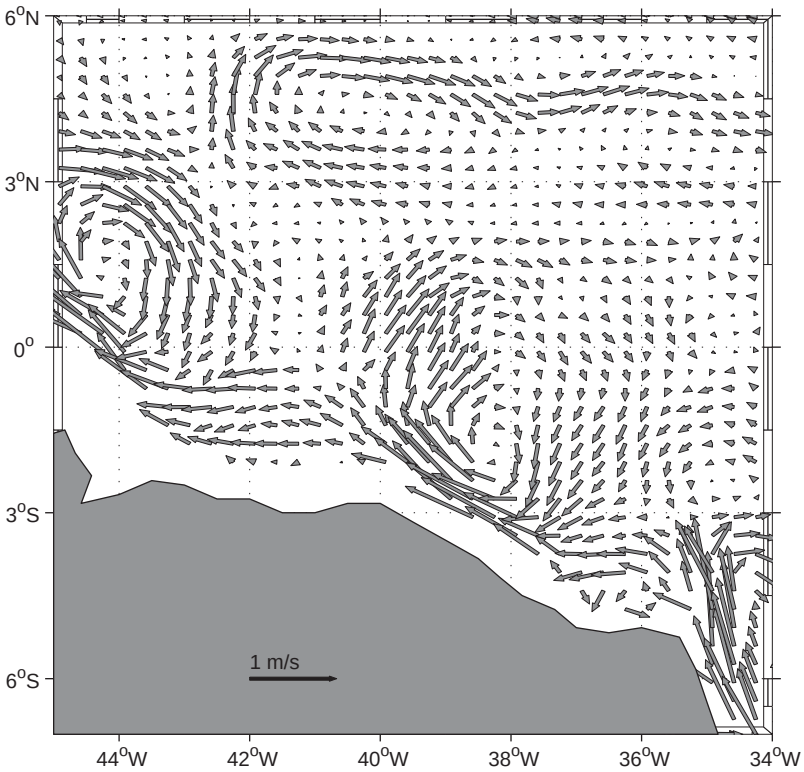

Fig. A.1. Upper panel (A.1 in text): Mapping results that use all data points from the simulation in the model region. Middle panel (A.2 in text): Mapping results that use data points from the simulation only at the observed sites shown in Fig. 1. Lower panel (A.3 in text): Difference in m/s between the vectors of A.1 and A.2.

the images only represent local and not remote influences.

(2) In this step, some areas of the coast are approximated by a line $y = ax + b$. The projection or the minimum distance between the positions of each velocity vector (x', y') to the line y is calculated. To do so, another line ($y_2 = (-1/a)x + b^2$) perpendicular to y that pass by x' is constructed. Both lines have one point in common where the lines cross, with coordinates (x_0, y_0). By simple geometry, the minimum distance from the point (x', y') to the line y is calculated by the following equation:

$$x' = (y_0 - b + x_0/a)/(1/a + a),$$

$$y' = (y_0 * a^2 + b + x_0 * a)/(1 + a^2).$$

The point is reflected into the coast by the expressions:

$$x_{\text{new}} = x_0 - 2(x_0 - x'),$$

$$y_{\text{new}} = y_0 - 2(y_0 - y').$$

(3) The vector from the observed data is reflected to the coastline. In order to do this each vector is taken as a complex number $v = u_0 + iv_0$. Than the components of the image vector are calculated as:

$$u_{\text{new}} = -\{u_0^2 + v_0^2\}^{1/2} * \cos(\theta + (\theta - a)),$$

$$v_{\text{new}} = -\{u_0^2 + v_0^2\}^{1/2} * \sin(\theta + (\theta - a)),$$

where $\alpha = \text{atan}(u_0/v_0)$ and $\theta = \text{atan}(a)$.

Owing to the sparse cruise data and the strong angular variation in the coastline, a different boundary condition was applied in the region where there are no images (coastline from 35°W–39°W). This boundary condition consists of removing regions with error greater than 0.1

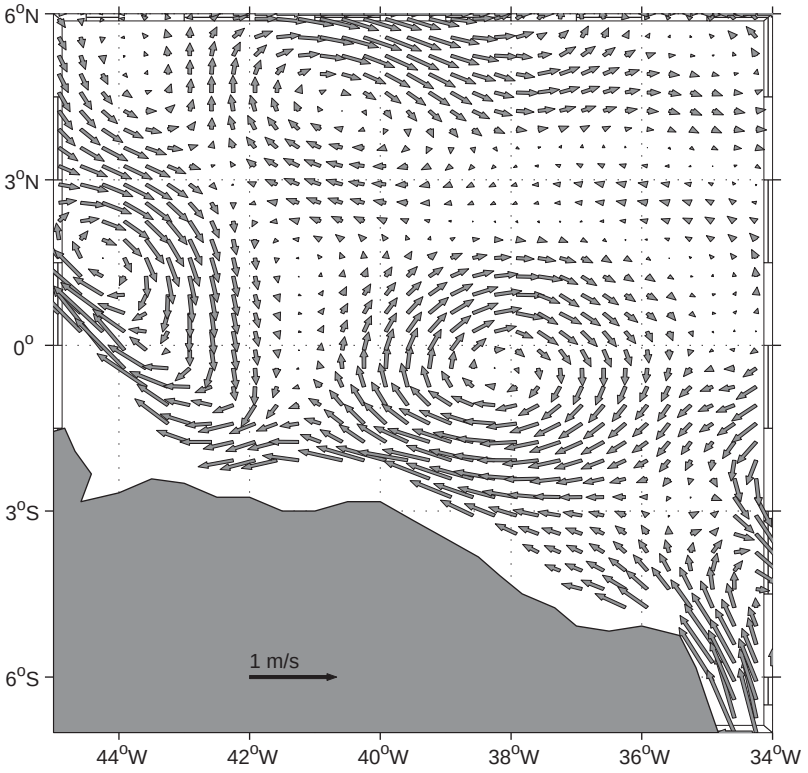

Fig. A.2.

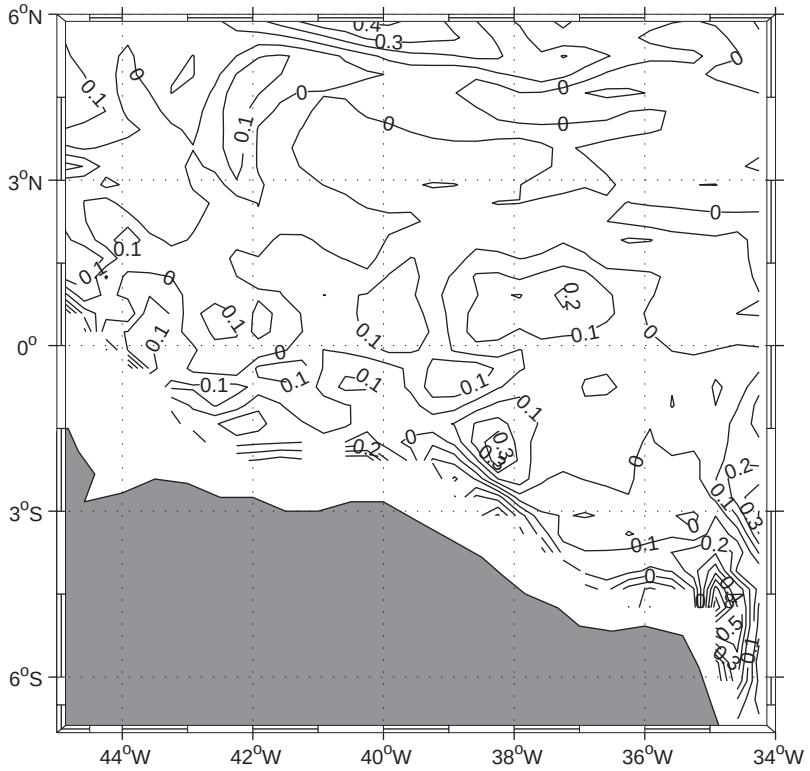

Fig. A.3.

and defining only one value of streamfunction along the coast. Then the gaps in the streamfunction field are interpolated again using a scalar OA with the same Gaussian function and parameters described above. The non-divergent u and v velocity components were calculated from the interpolated streamfunction field.

In order to validate the OA method for the sparse data in the study area a test was conducted using results from a numerical model. The model is not described, as we are only interested in a model result for testing the OA method. The model output selected was from February 15, 2002 and a depth of 230 m. These outputs were interpolated to the same positions as the cruise stations, simulating a "model cruise". Then the OA procedure was applied to the "model cruise", generating a velocity field at the model grid.

The original model output and the "model cruise" interpolated field were compared. Fig. A.1,model output,and A.2, model cruise output, show that the mean features of the circulation of the region were well reproduced. The differences between the two fields (original and interpolated) are given in Fig. A.3. Over most of the region, errors were less than 20 cm/s. The regions with highest errors are close to the western boundary: at 35°W and 38°W, where the errors range from 40 cm/s to 60 cm/s. At 38°W, the errors are large due to the paucity of the data in this region. At 35°W, the large variability is excessively smoothed because of the decorrelation scale selected.

References

Anderson, D.L.T., Corry, R.A., 1985. Seasonal transport variations in the Florida Straits: a model study. Journal of Physical Oceanography 15, 773–786.

Bourles, B., Gouriou, Y., Chucla, R., 1999a. On the circulation in the upper layer in the western equatorial Atlantic. Journal of Geophysical Research 104, 21151–21170.

Bourles, B., Molinari, R.L., Johns, E., Wilson, W.D., Leaman, K.D., 1999b. Upper layer currents in the western tropical North Atlantic (1989–1991). Journal of Geophysical Research 104, 1361–1376.

Bretherton, F.P., Davis, R.E., Fandry, C.B., 1976. A technique for objective analysis and design of oceanographic experiments applied to MODE-73. Deep-Sea Research 23, 559–582.

Cochrane, J., Kelly, F., Olling, C., 1979. Subthermocline countercurrents in the western equatorial Atlantic Ocean. Journal of Physical Oceanography 9, 724–738.

da Silveira, I.C.A., Brown, W.S., Flierl, G.R., 2000. Dynamics of the North Brazil Current retroflection region from the Western Tropical Atlantic Experiment observations. Journal of Geophysical Research 105, 28,559–28,583.

Firing, E., Ranada, J., Caldwell, P., 1995. Processing ADCP Data with the CODAS Software System, Version 3.1. Technical Report, University of Hawaii, Honolulu, Hawaii, unpublished.

Garzoli, S.L., Ffield, A., Johns, W.E., Ya, Q., 2004. North Brazil Current retroflection and transports. Journal of Geophysical Research 62.

Gordon, A.L., 1986. Interocean exchange of thermocline water. Journal of Geophysical Research 91, 5037–5046.

Johns, W.E., Lee, T.N., Beardsley, R., Candela, J., Castro, B., 1998. Annual cycle and variability of the North Brazil Current. Journal of Physical Oceanography 28, 103–128.

Kurgansky, M.V., Budillon, G., Salusti, E., 2002. Tracers and potential vorticities in ocean dynamics. Journal of Physical Oceanography 32, 3562–3577.

Mayer, D.A., Weisberg, R.H., 1993. A description of COADS surface meteorological fields and the implied Sverdrup transports for the Atlantic Ocean from 30°S to 60°N. Journal of Physical Oceanography 23, 2201–2221.

Merle, J., 1978. Atlas Hydrologique Saisonnier de L'Ocean Atlantique Intertropical. Travaux et Documents de L'O.R.S.T.O.M., No 82, O.R.S.T.O.M., Paris.

Millero, F.J., Poisson, A., 1981. International one-atmosphere equation of state of seawater. Deep-Sea Research 28A, 625–629.

Molinari, R.L., Bauer, S., Snowden, D., Johnson, G., Bourles, B., Gouriou, Y., Mercier, H., 2003. A comparison of kinematic evidence for tropical cells in the Atlantic and Pacific oceans. In: Goni, G., Malanotte-Rizzoli, P. (Eds.), Interhemispheric Water Exchange in the Atlantic Ocean. Elsevier, Amsterdam, pp. 269–286.

Muller, P., 1995. Ertel's potential vorticity theorem in physical oceanography. Review of Geophysics 33, 67–97.

Rhines, P.B., 1986. Vorticity dynamics of the oceanic general circulation. Annual Review of Fluid Mechanics 18, 433–497.

Schott, F., Boening, C.W., 1991. Evaluation of the WOCE model in the western equatorial Atlantic. Journal of Geophysical Research 96, 6993–7004.

Schott, F., Stramma, L., Fischer, J., 1995. The warm water inflow into the western tropical Atlantic boundary regime, spring 1994. Journal of Geophysical Research 100, 24745–24760.

Schott, F., Fisher, J., Stramma, L., 1998. Transports and pathways of the upper-layer circulation in the western tropical Atlantic. Journal of Physical Oceanography 28, 1904–1928.

Schott, F., Brandt, P., Hamman, M., Fisher, J., Stramma, L., 2002. On the boundary flow off Brazil at 5–10°S and its connection to the interior tropical Atlantic. Geophysical Research Letters 29.

Schott, F., Dengler, M., Brandt, P., Affler, K., Fischer, J., Bourles, B., Gouriou, Y., Molinari, R.L., Rhein, M., 2003. The zonal currents and transports at 35°W in the tropical Atlantic. Geophysical Research Letters 30.

Sippican, 1991. MK-12 Oceanographic Acquisition System, Technical Manual R2626. Sippican Incorporated, Marion, Massachusetts, unpublished.

Snowden, D., Molinari, R.L., 2003. Subtropical cells in the Atlantic Ocean: an observations summary. In: Goni, G., Malanotte-Rizzoli, P. (Eds.), Interhemispheric Water Exchange in the Atlantic Ocean. Elsevier, Amsterdam, pp. 287–312.

Stramma, L., Schott, F., 1996. Western equatorial circulation and interhemispheric exchange. In: Krauss, W. (Ed.), The Warmwatersphere of the North Atlantic Ocean. Gebruder Borntraeger, pp. 195–225.

Tsuchiya, M., 1986. Thermostads and circulation in the upper layer of the Atlantic Ocean. Progress In Oceanography 16, 235–267.

Zhang, D., McPhaden, M.J., Johns, W., 2003. Observational evidence for flow between the subtropical and tropical Atlantic: the Atlantic Subtropical Cells. Journal of Physical Oceanography 33, 1783–1797.